


## Spontaneous separation of attractive chiral mixtures

Jia-jian Li , Rui-xue Guo, and Bao-quan Ai\*

*Key Laboratory of Atomic and Subatomic Structure and Quantum Control (Ministry of Education), Guangdong Basic Research Center of Excellence for Structure and Fundamental Interactions of Matter, School of Physics, South China Normal University, Guangzhou 510006, China*

*and Guangdong Provincial Key Laboratory of Quantum Engineering and Quantum Materials, and Guangdong-Hong Kong Joint Laboratory of Quantum Matter, South China Normal University, Guangzhou 510006, China*

 (Received 22 March 2024; revised 27 June 2024; accepted 1 August 2024; published 26 August 2024)

The separation of chiral matter has garnered significant attention due to its wide-ranging applications in biological and chemical processes. In prior researches, particle interactions were predominantly repulsive, but the indiscriminate attraction among particles under attractive interactions makes the separation of mixtures more difficult. The question of whether chiral mixed particles, characterized by attractive effects, can undergo spontaneous separation, remains unresolved. We study a binary mixture of chiral (counterclockwise or clockwise) active particles with attractive interactions. It is demonstrated that attractive chiral particles can undergo spontaneous separation without the aid of any specific strategies. The key factor driving the separation is the attractive interactions, enabling the formation of stable clusters of particles with same chirality. There exist optimal parameters (self-propelled velocity, angular velocity, and packing fraction) at which the separation is optimal. Our results may contribute to a deeper understanding of the mechanisms behind chiral matter separation and potentially catalyze further experimental investigations in this field.

DOI: [10.1103/PhysRevE.110.024608](https://doi.org/10.1103/PhysRevE.110.024608)

### I. INTRODUCTION

In recent years, active matter has garnered significant attention from physicists, as the injection of external energy drives these systems far from equilibrium [1], leading to a range of intriguing phenomena such as directional transport [2–11], mobility-induced phase separation (MIPS) [12–15], glassy dynamics [16,17], flocking transitions [18–26], and so on. These findings are of crucial importance for understanding various biological and chemical scenarios, as well as for designing microscale devices. A fundamental example of active matter is particles with self-propulsion capabilities, where changes in their direction of motion are typically driven by thermal fluctuations and remain unbiased. Interestingly, when the translational motion with self-propulsion and rotational motion are coupled in chiral matter (where chirality originates from chiral shape or propulsion symmetry breaking), they give rise to trajectories resembling circular motion in two dimensions (or helices in three dimensions). Such active chiral motion is widely observed in biological and chemical matter, such as bacteria [27–30], malaria parasites [31], helically swimming sperm cells [32–34], chiral microtubules [35], shape-asymmetric colloidal [7,36,37], and granular ellipsoids [38,39]. A plenty of peculiar phenomena in chiral matter systems are becoming increasingly captivating [40], which includes collective behaviors [41–46], odd viscosity [47–51], active turbulence and vortices [50–53], hyperuniform states [54], and separation of mixtures [38,55–67].

The separation of chiral mixtures holds significant potential in various fields such as bioengineering and chemical engineering. This is particularly true in two-dimensional space, where opposite chirality results in entirely contrasting kinetic behaviors (clockwise or counterclockwise rotation), thus offering a robust basis for mixture separation. Reported separation of chiral mixtures requires the presence of extra special interactions or specific external manipulations [38,55–66]. Examples of the former include the separation of particles with opposite chirality under explicit alignment interactions [55–57], the spinodal decomposition of gearlike particles leading to phase separation [58,59], the self-sorting of active semiflexible filaments caused by intrinsic curvature [60], and demixing of binary mixtures induced by hydrodynamical interactions [61]. Examples of the latter include well-designed geometric constraints such as chiral flower patterns [62], asymmetric pattern arrays [63], polarized wall currents [64], and periodic potentials [38], as well as external driving forces like shear flow [65] and convective roll arrays [66]. In addition, the chiral mixture can be separated with the assistance of the local alignment effect induced by MIPS [67]. In the earlier mentioned separation system of chiral mixed particles, the interactions between particles are purely repulsive. However, in practical systems, attractive interactions [26,68,69] are also commonly present. Due to these attractive forces between particles, different types of particles tend to tightly bind together, thereby making their separation very difficult. Therefore, whether chiral mixed particles with attractive interactions can spontaneously separate without the assistance of external strategies remains an unanswered question.

\*Contact author: [aibq@scnu.edu.cn](mailto:aibq@scnu.edu.cn)

To answer this question, we investigated the segregation of binary mixture of active chiral particles with attractive interactions. It is found that particles of opposite chirality can spontaneously segregate without the need for any special interactions (such as alignment interactions) or external manipulation. The core mechanism behind this is the attractive interactions, which leads to the clustering of particles with same chirality. The segregation coefficient exhibits a peak function concerning the self-propelled velocity, angular velocity, and packing fraction, with an optimal parameter range that maximizes the degree of segregation. Our work proposes a different mechanism for the spontaneous segregation of attractive chiral particles, which will provide a theoretical foundation for the experiments related to the demixing of chiral matter.

## II. MODEL AND METHODS

We consider a binary mixture system composed of  $N$  chiral self-propelled particles [50% counterclockwise (CCW) and 50% clockwise (CW) particles] with diameter  $\sigma$  in a two-dimensional  $L \times L$  box under periodic boundary conditions. The dynamics of each particle is characterized by its central position  $r_i \equiv (x_i, y_i)$  and its polarity vector  $n_i \equiv (\cos \theta_i, \sin \theta_i)$ , where  $\theta_i$  is the orientation. The orientation is determined by rotational diffusion and a constant torque. Therefore, the dynamics of particle  $i$  can be described by the following equations:

$$m\ddot{r}_i = -\gamma\dot{r}_i + F_i + \gamma v_0 n_i + \gamma\sqrt{2D_0}\xi_i(t), \quad (1)$$

$$\dot{\theta}_i = q_i\Omega + \sqrt{2D_r}\eta_i(t), \quad (2)$$

where  $m$  is the mass;  $\gamma$  is the friction coefficient;  $v_0$  denotes the self-propulsion speed;  $D_0$  and  $D_r$  represent the translational diffusion coefficient and rotational diffusion coefficient, respectively; and  $\xi_i(t)$  and  $\eta_i(t)$  are Gaussian white noises with unit variance with zero mean. The constant angular velocity  $\Omega$  originates from the torque suffered by the particles, which proceeds a circular motion with orbital radius  $R = v_0/\Omega$ . The two directions that distinguish chiral motion are represented by  $q = \pm 1$ , where  $q = 1$  corresponds to the CCW particles and  $q = -1$  corresponds to the CW particles.

The interactions between particles are modeled by the Lennard-Jones potential, which reads  $U_{LJ}(r) = 4\varepsilon[(\sigma/r)^{12} - (\sigma/r)^6]$  for  $r \leq 3\sigma$  and zero otherwise;  $\varepsilon$  is the interaction strength. Note that such a selection of the cutoff distance allows for the presence of attractive interactions between particles when the distance exceeds  $2^{1/6}\sigma$ . Thus, the force is  $F_i = -\nabla_i U$ , where  $U = \sum_{i < j} U_{LJ}(|r_i - r_j|)$ .

In order to quantify the degree of demixing between the two types of particles, a segregation coefficient  $S$  based on the Voronoi tessellation has been introduced [70],

$$S = \left\langle \frac{1}{N} \sum_{i=1}^N 2 \left( \frac{n_i^s}{n_i^t} - \frac{1}{2} \right) \right\rangle, \quad (3)$$

where  $n_i^s$  represents the number of particles in the neighborhood of particle  $i$  that belong to the same species as it and  $n_i^t$  represents the total number of neighbors of particle  $i$ . The brackets  $\langle \dots \rangle_t$  denote a time average. By definition,

$S = 1$  corresponds to complete demixing, whereas  $S = 0$  corresponds to complete mixing.

To quantify the hidden velocity alignment in a system with attractive interactions, we define a spatial correlation function of the velocity direction [71],

$$Q(r) = \frac{1}{N} \sum_{i=1}^N Q_i(r), \quad (4)$$

where  $Q_i(r) = 1 - 2 \sum_j d_{ij}/(\pi M_k)$ ;  $d_{ij}$  is the angular distance between the velocity angle  $\phi_i$  (respect to the  $x$  axis) of particle  $i$  and the velocity angle  $\phi_j$  of its neighbors within radius  $r$ , obtained by  $\min\{|\phi_i - \phi_j|, 2\pi - |\phi_i - \phi_j|\}$ ;  $M_k$  is the number of particles in the circle shell with radius  $r$ ; and  $Q(r) = 1$ ,  $Q(r) = -1$  and  $Q(r) = 0$  mean perfect velocity alignment, antiveloccity alignment and no velocity alignment, respectively.

We numerically integrate Eqs. (1) and (2) using the stochastic Euler algorithm with a time step  $\Delta t = 10^{-3}$  and a total time  $t_{\text{total}} = 10^5$ . Initially, the two types of particles are uniformly mixed and randomly distributed within the box, with their orientational angles selected randomly from the range  $[0, 2\pi]$ . The system undergoes such a  $t_{\text{total}}$  sufficient to reach a nonequilibrium steady state, after which we perform a time average of the separation coefficient over an additional  $1000\tau$  ( $\tau = 2\pi/\Omega$ ). The packing fraction is defined as  $\Phi = N\pi\sigma^2/(4L^2)$ . We set  $\varepsilon = 0.6$  to get a moderate strength of attractive interactions. Unless otherwise stated, the following simulation results are obtained under the parameter sets  $m = 1.0$ ,  $\gamma = 1.0$ ,  $D_r = 10^{-4}$ , and  $D_0 = 10^{-7}$ .

## III. RESULTS AND DISCUSSION

To effectively separate two types of particles, two general conditions need to be met. First, there must be noticeable distinctions in the motion behaviors between the two particle types. In our system, consisting of particles with different chirality, they move in circular paths in opposing directions, thus satisfying the first condition. Second, particles of the same type gather while those of different types disperse, resulting in the formation of stable clusters for each particle type. This often requires explicit alignment interactions [55–57], which are absent in our system.

However, a recent study has found that active Brownian particle systems with attractive interactions can undergo a flocking transition without explicit alignment interactions [26]. The mechanism involves the attractive interactions inducing active particles to form stable pairs, leading to local velocity alignment, and, subsequently, the attractive interactions between aligned small clusters give rise to aligned large clusters. This phenomenon nicely satisfies the second condition required for particle separation, making particle separation achievable in our system.

To specifically investigate the separation mechanism of binary chiral attractive particles, we explore the separation dynamics under variations in self-propulsion speed  $v_0$ , angular velocity  $\Omega$ , and packing fraction  $\Phi$ .

Figure 1 illustrates the typical snapshots of the binary mixture consisting of 1000 CCW particles and 1000 CW particles for different angular velocity  $\Omega$  at  $v_0 = 2.5$  and

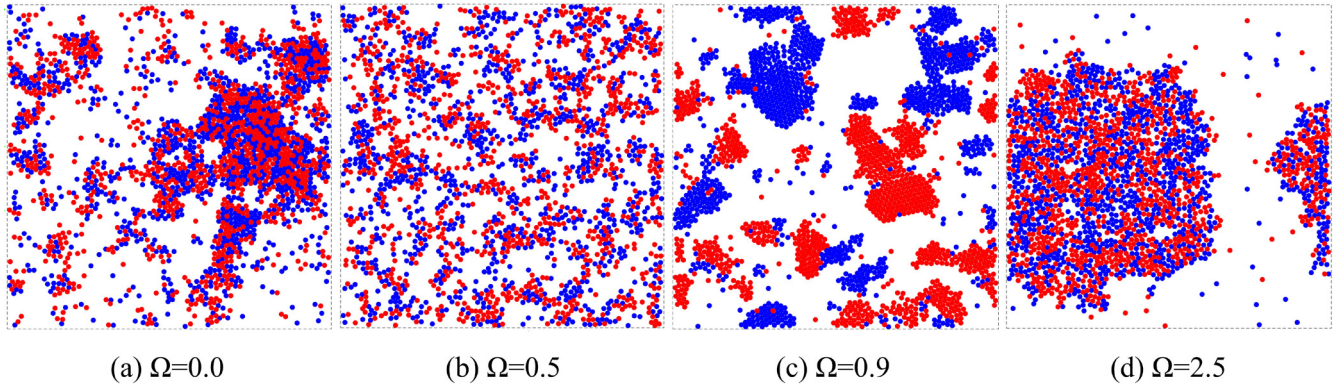


FIG. 1. Typical snapshots of the binary system of 1000 CCW particles (blue disks) and 1000 CW particles (red disks) for different  $\Omega$  at  $v_0 = 2.5$  and  $\Phi = 0.27$ .

$\Phi = 0.27$ . When  $\Omega = 0$ , the chirality difference is absent, and the two types of particles are indistinguishable, making demixing impossible [as shown in Fig. 1(a)]. The presence of attractive interactions leads to local alignment of active particles within a very small range [as shown in Fig. 2(a)]. Note that the flocking state reported by Ref. [26] has vanished at  $v_0 = 2.0$ , so only very weak local alignment is present in our system with  $v_0 = 2.5$ . When the angular velocity takes a relatively small value (e.g.,  $\Omega = 0.5$ ), although there is chirality difference, the attractive interaction cannot take effect under large-radius circular motion ( $R > 3\sigma$ ), leading to the disappearance of local alignment [as shown in Fig. 2(b)]. This prevents particles of the same chirality from forming stable clusters [as shown in Fig. 1(b)], and the two types of particles remain inseparable. When the angular velocity takes an intermediate value (e.g.,  $\Omega = 0.9$ ), the radius of circular motion satisfies  $2^{1/6}\sigma < R < 3\sigma$ , for which the attractive interactions are significant and local alignment is strong [as shown in Fig. 2(c)]. Particles within the range  $2^{1/6}\sigma < r < 3\sigma$ , regardless of whether they have the same chirality, will form pairs due to attraction and exhibit local alignment. If particles of the same type come into contact, then they cluster and rotate in the same direction due to local alignment [as shown in Figs. 3(a) and 3(b)]. If particles of different types collide, then their opposite chirality causes them to rotate in opposite directions, leading to spatial separation [as shown in Fig. 3(c)]. With both distinct chirality and the ability of

same-type particles to form stable local clusters, we observe the separation of the two types of particles, each forming small clusters that collectively undergo circular motion [as shown in Fig. 1(c)]. The process of cluster formation described above readily evokes the concept of odd viscosity [49], which results in radial compression and increased density of particles of the same chirality. We propose that odd viscosity enhances the binding of particles of the same chirality, thereby promoting the separation of particles of opposite chirality. Due to constraints imposed by the single-particle circular motion radius, it is challenging for clusters of the same type to combine into stable larger clusters. In other words, as the cluster size increases, outer particles require greater linear velocity to remain within the cluster. However, particle linear velocity is limited ( $\leq v_0$ ). When the cluster size significantly exceeds the radius  $R$  of circular motion of particles in their free state, outer particles cannot stably follow the cluster. To demonstrate this, we included a probability distribution plot of cluster sizes  $r_c$  (as shown in Fig. 4), where the curve exhibits a sharp decline at  $r_c \approx R$ . When the angular velocity takes a relatively large value (e.g.,  $\Omega = 2.5$ ), particles undergo circular motion with a very small radius, for which self-propulsion is neglectable and the generation of local alignment is hindered [as shown in Fig. 2(d)]. Consequently, the two types of particles are mixed [as shown in Fig. 1(d)].

The local alignment can be quantified by the corresponding spatial velocity correlation function  $Q(r)$  which is displayed

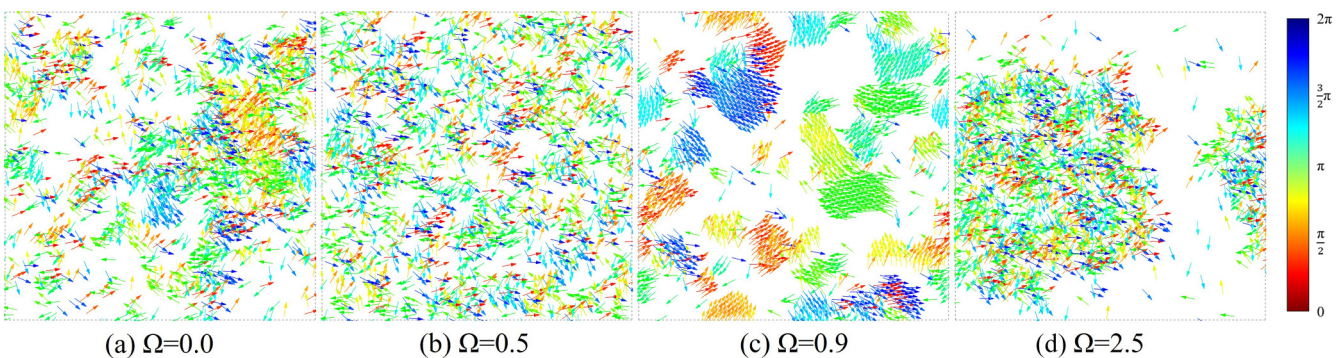


FIG. 2. The velocities of particles for typical snapshots in Fig. 1. The color on the velocity vector represents the mapping of velocity direction angles.



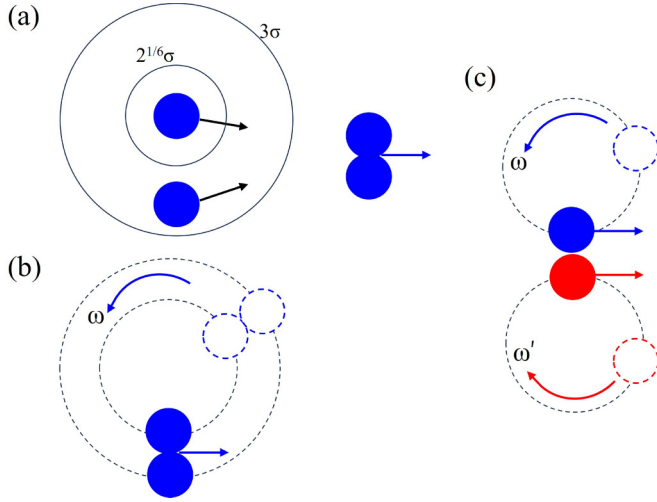


FIG. 3. Sketch of the mechanism of the segregation. (a) Particles within the attraction range attract each other and undergo local velocity alignment. (b) Particles with the same chirality maintain alignment and collectively perform circular motion. (c) Particles with opposite chirality perform circular motion with opposite angular velocities after align, leading to alignment disruption and separation of the two particles.

in Fig. 5(a). The  $Q(r)$  for  $\Omega = 0$  is slightly stronger than the  $Q(r)$  for both smaller (e.g.,  $\Omega = 0.5$ ) and larger (e.g.,  $\Omega = 2.5$ ) angular velocities, indicating that the local alignment for  $\Omega = 0$  is slightly stronger than in the latter two cases. It should be noted that when a tailored intermediate value of angular velocity (e.g.,  $\Omega = 0.9$ ) is chosen, the velocity correlation function and correlation length noticeably increase, suggesting the presence of significant local alignment in the system. Figure 5(b) shows the number of clusters  $\langle N_{\text{cluster}} \rangle$  and max size of clusters  $\langle r_{c,\text{max}} \rangle$  versus angular velocity  $\Omega$  at  $v_0 = 2.5$ . When  $\Omega$  increases,  $\langle r_{c,\text{max}} \rangle$  undergoes twice decrease followed by increase, corresponding to  $\langle N_{\text{cluster}} \rangle$  experiencing twice

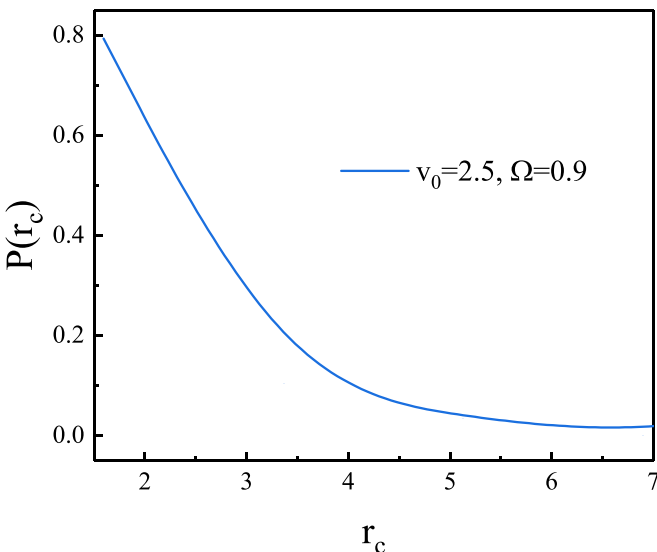


FIG. 4. Probability distribution of cluster sizes  $r_c$  at  $v_0 = 2.5$ ,  $\Omega = 0.9$ , and  $\Phi = 0.27$ .

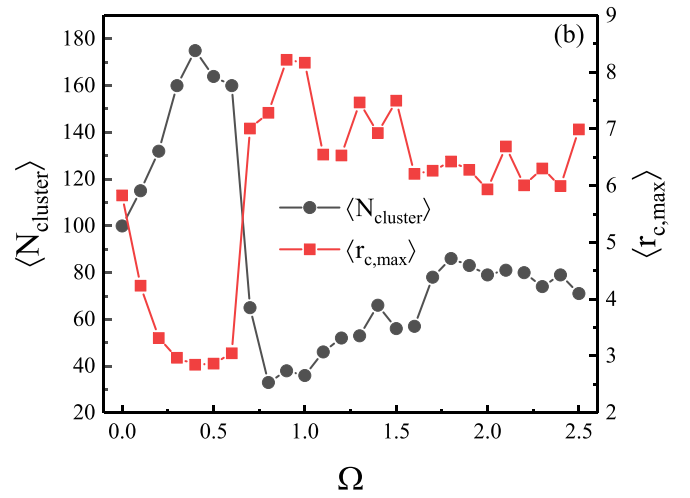
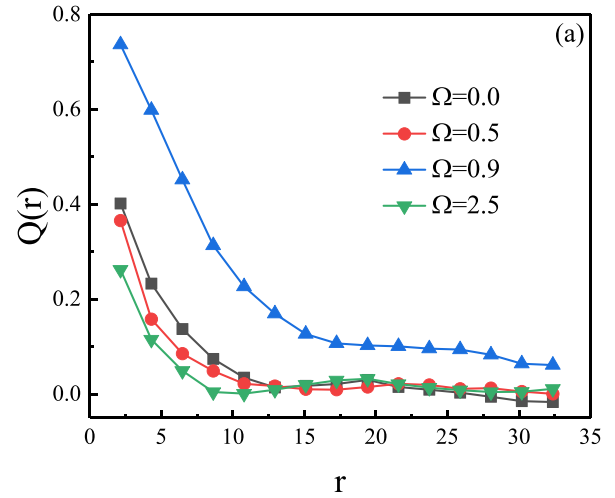


FIG. 5. (a) The spatial velocity correlation function  $Q(r)$  versus the distance  $r$  for typical snapshots shown in Figs. 1(a)–1(d). (b) The number of clusters and size of max cluster as functions of angular velocity  $\Omega$  at  $v_0 = 2.5$ .

increase followed by decrease. The first phase occurs because the particle's circular motion radius  $R$  is significantly larger than the range where attraction dominates, enhancing chiral motion and weakening local alignment, thereby reducing cluster stability. If  $\Omega$  continues to increase, then  $R$  approaches and falls within the dominance range of attraction, leading to pronounced separation where particles of the same chirality form stable clusters. The second phase occurs because  $R$  is smaller than the dominance range of attraction, weakening both local alignment and separation phenomena. Further increasing  $\Omega$  renders self-propulsion negligible, local alignment completely disappears, and particles aggregate to form a large circular cluster resembling attractive passive particles.

Figure 6(a) plots the separation coefficient  $S$  as a function of angular velocity  $\Omega$  for different values of  $v_0$  at  $\Phi = 0.27$ , which quantifies the degree of separation between the two types of particles.  $S$  initially increases with increasing  $\Omega$  and then decreases. There exists an optimal angular velocity  $\Omega_{\text{op}}$  that maximizes the degree of demixing. When  $\Omega \rightarrow 0$ , both types of particles exhibit infinite radii (i.e., linear motion), and their dynamic behaviors become identical. Consequently, they

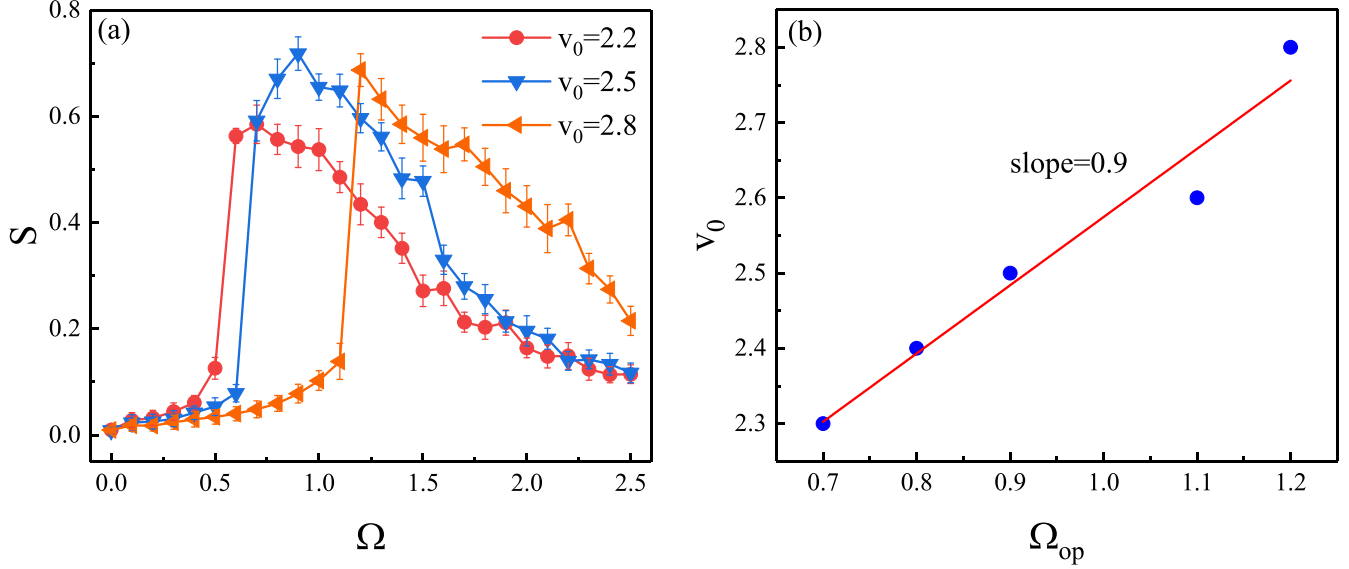


FIG. 6. (a) The dependence of separation coefficient  $S$  on angular velocity  $\Omega$  for different  $v_0$  at  $\Phi = 0.27$ . (b) Self-propulsion speed  $v_0$  as a function of the optimal angular velocity  $\Omega_{op}$ , which is a linear function with slope = 0.9.

cannot separate and  $S \rightarrow 0$ . When  $\Omega \rightarrow \infty$ , the radii of particle circular motion approach zero, rendering self-propulsion almost ineffective, and causing the loss of local alignment. Thus, neither type of particles is able to form stable clusters and  $S \rightarrow 0$ . When  $\Omega$  takes an appropriate intermediate value, the two types of particles exhibit significant dynamic differences, with attractive interactions dominating within the radius range of particle circular motion ( $2^{1/6}\sigma < R < 3\sigma$ ). Therefore, under the contribution of local alignment, the two types of particles can separate and form clusters, even resulting in the maximum value of  $S$  ( $\Omega = \Omega_{op}$ ). Furthermore, we observe that with an increase in  $v_0$ , the position of peak shifts towards higher values of angular velocity. Figure 6(b) illustrates the dependence of self-propulsion speed  $v_0$  on the optimal angular velocity  $\Omega_{op}$ , revealing an approximate linear relationship (slope = 0.9). The linear relationship between  $v_0$  and  $\Omega_{op}$  arises from the necessity for the optimal separation state to occur when the particle's circular motion radius ( $R = v_0/\Omega$ ) aligns with the value where interparticle attractive interactions dominate. Thus, as  $v_0$  increases,  $\Omega_{op}$  must also approximately increase linearly to ensure the resulting radius matches the dominance of attractive forces.

Figure 7 displays the function of the separation coefficient  $S$  versus the self-propulsion speed  $v_0$  for different  $\Omega$  at  $\Phi = 0.27$ . One can observe that  $S$  is a peak function with respect to  $v_0$ . When  $v_0$  is small, the particles have smaller motion radii, resulting in insignificant self-propulsion and weak local alignment [as shown in Fig. 8(a)], so  $S$  is small. When  $v_0$  is very large, on the one hand, both types of particles tend towards linear motion, leading to a less pronounced chirality difference; on the other hand, larger self-propulsion force makes it easier for them to break away from clusters and break the local alignment [as shown in Fig. 8(a)], which is detrimental to separation, thus causing  $S$  to tend towards zero. Moreover, the position of the peak shifts to the right with increasing angular velocity  $\Omega$ . Figure 8(b) plots the number of clusters

( $\langle N_{cluster} \rangle$ ) and size of the max cluster ( $r_{c,max}$ ) as functions of self-propulsion speed  $v_0$  at  $\Omega = 1.0$ . Around  $v_0 = 2.8$ , the separation coefficient  $S$  sharply decreases accompanied by a sudden decrease in  $\langle r_{c,max} \rangle$  (or a sharp increase in  $\langle N_{cluster} \rangle$ ).

We plot the phase diagram of the separation coefficient  $S$  in the  $\Omega - v_0$  representation at  $\Phi = 0.27$  in Fig. 9. Both excessively large or small self-propulsion speed  $v_0$  and angular velocities  $\Omega$ , are unfavorable for demixing to occur, and particles with larger  $\Omega$  require larger  $v_0$  to realize separation. This is because, on the one hand, the two types of particles require a noticeable chirality difference, and on the other hand, they also need appropriate motion radii (i.e., a combination of appropriate  $v_0$  and  $\Omega$ ) for local alignment to take place, thereby enabling the formation of stable clusters.

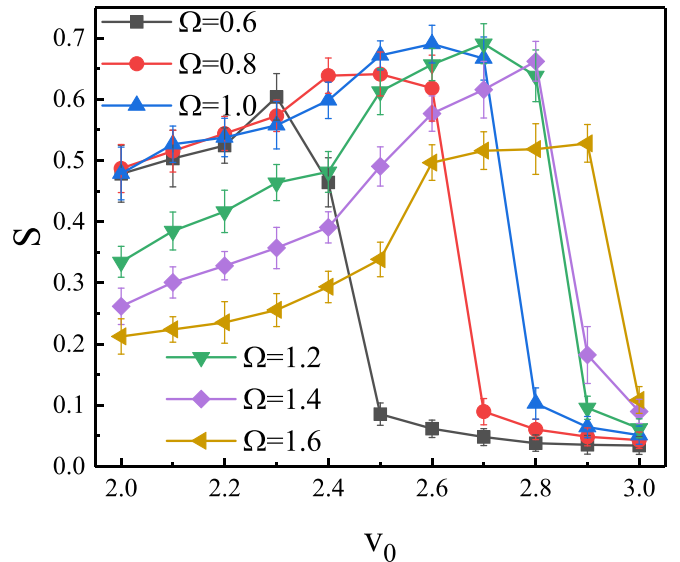


FIG. 7. Separation coefficient  $S$  as a function of self-propulsion speed  $v_0$  for different  $\Omega$  at  $\Phi = 0.27$ .

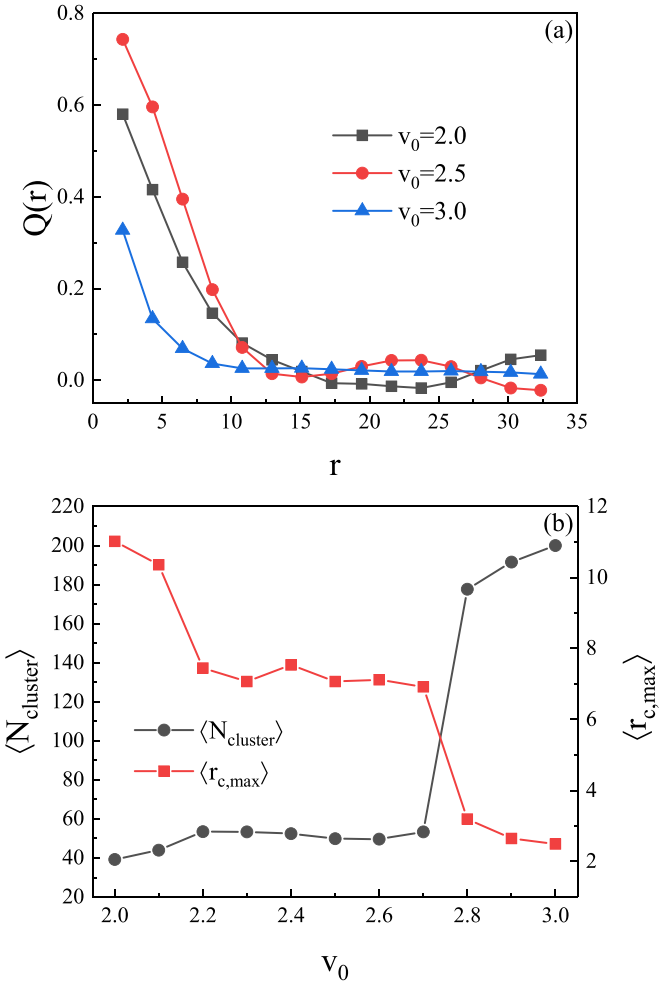


FIG. 8. (a) The spatial velocity correlation function  $Q(r)$  versus the distance  $r$  for different self-propulsion speed  $v_0$  at  $\Omega = 1.0$ . (b) The number of clusters and size of max cluster as functions of self-propulsion speed  $v_0$  at  $\Omega = 1.0$ .

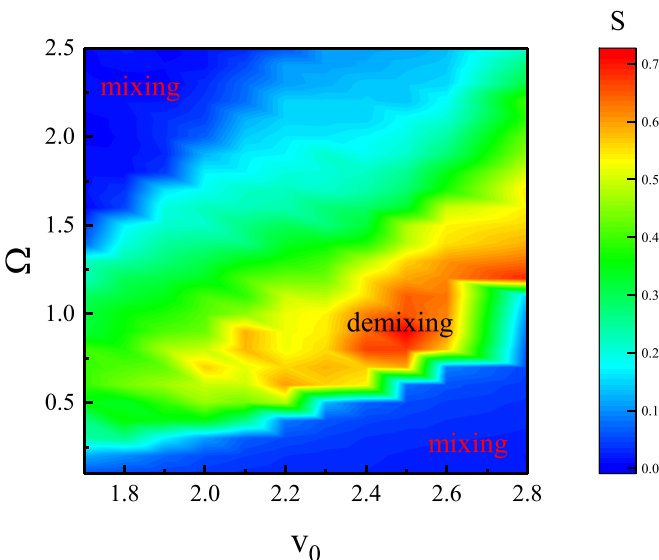


FIG. 9. Phase diagram of the separation coefficient  $S$  in the  $\Omega - v_0$  representation at  $\Phi = 0.27$ .

The typical snapshots of the binary mixture consisting of 1000 CCW particles and 1000 CW particles for different packing fraction  $\Phi$  at  $v_0 = 2.5$  and  $\Omega = 0.9$  are shown in Fig. 10, where  $\Phi$  is altered by changing the size of the box  $L$ , and the snapshots are all scaled from their actual sizes to a standardized image dimension. When the packing fraction is very small (e.g.,  $\Phi = 0.03$ ), the particles are widely spaced apart [shown in Fig. 10(a)], resulting in weak interactions and therefore limited local alignment [shown in Fig. 11(a)]. Consequently, even if the two types of particles exhibit significant dynamical differences, they are unable to form distinct clusters individually, thus hampering demixing. Furthermore, the particles can only form small clusters with nearby neighbors under the influence of attraction, and these small clusters can only undergo circular motion within a small range, thus even with prolonged time, they cannot merge with other clusters whose distance is much greater than the circular motion radius. To prove that the cluster evolution has reached a steady state, we calculated the evolution of cluster number and maximum cluster size over time, which shows in Appendix. When the packing fraction is at an intermediate value (e.g.,  $\Phi = 0.21$  and  $\Phi = 0.27$ ), the distance between particles is moderate [as shown in Fig. 10(b) and 10(c)], promoting strong local alignment due to prevailing attractive interactions [shown in Figs. 11(b) and 11(c)]. As a result, clusters of the same type of particles are formed when encountering each other due to the alignment effect, while particles of different types separate when their rotation directions are opposite, leading to a clear separation of the two types of particles. When the packing fraction is very large (e.g.,  $\Phi = 0.5$ ), the distance among particles becomes too small [shown in Fig. 10(d)], leading to predominant repulsive interactions and limited occurrence of local alignment [shown in Fig. 11(d)]. Thus, clusters of the same type of particles cannot form stably, preventing demixing from occurring. Furthermore, in mixtures, particles of opposite chirality counteract each other, leading to the alternation of tiny vortices forming and dissipating over time, with weak spatial correlation, resembling turbulent phenomena.

Figure 12(a) depicts the corresponding spatial velocity correlation function  $Q(r/L)$  for different packing fraction  $\Phi$  at  $v_0 = 2.5$  and  $\Omega = 0.9$ , which quantitatively assess the degree of local alignment. For cases where particle distribution is sparse (e.g.,  $\Phi = 0.03$ ) or dense (e.g.,  $\Phi = 0.5$ ), local alignment is weak, resulting in a smaller and faster decaying  $Q(r/L)$ . However, for an appropriate packing fraction (e.g.,  $\Phi = 0.21$  and  $\Phi = 0.27$ ), particles exhibit stronger local alignment capability, leading to a larger  $Q(r/L)$ . Figure 12(b) shows the number of clusters  $N_{\text{cluster}}$  and size of the max cluster  $\langle r_{c,\text{max}} \rangle$  as functions of packing fraction  $\Phi$  at  $v_0 = 2.5$  and  $\Omega = 0.9$ . It can be observed that  $\langle r_{c,\text{max}} \rangle$  initially increases and then decreases with increasing  $\Phi$ , while  $\langle N_{\text{cluster}} \rangle$  decreases initially and then increases. This phenomenon arises because increasing  $\Phi$  initially facilitates easier interactions between particles, but as  $\Phi$  becomes very large, the interparticle distances become small such that attractive interactions no longer dominate. This increases the difficulty for particles to form large clusters.

Figure 13 illustrates the dependence of the separation coefficient  $S$  on the packing fraction  $\Phi$  for different



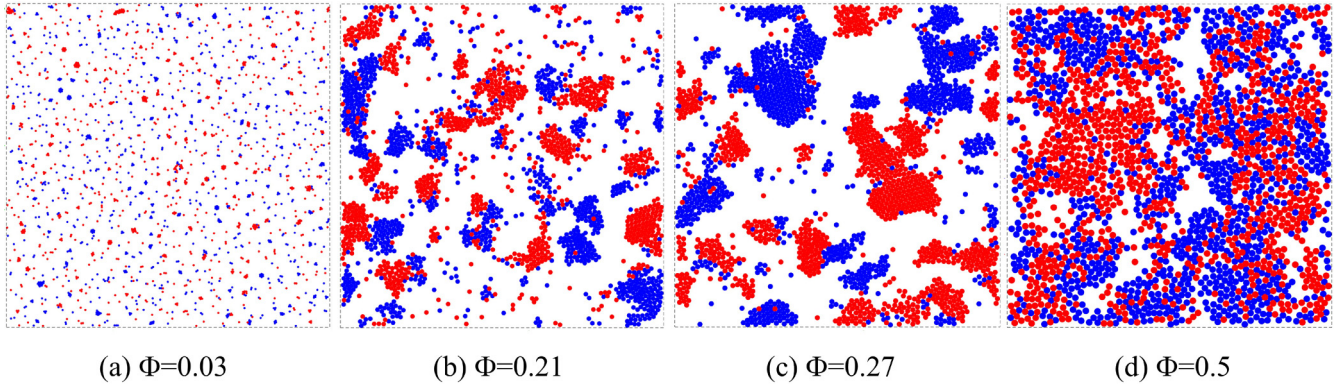


FIG. 10. Typical snapshots of the binary system of 1000 CCW particles (blue disks) and 1000 CW particles (red disks) for different  $\Phi$  at  $v_0 = 2.5$  and  $\Omega = 0.9$ . The snapshots are all scaled from their actual sizes to a standardized image dimension.

self-propulsion speed  $v_0$  at  $\Omega = 0.9$ . It is found that  $S$  first increases and then decreases with the increase in  $\Phi$ , and there is an optimal packing fraction where separation coefficient gets its maximum. When  $\Phi \rightarrow 0$ , the particle distribution is so sparse that their interactions are not significant, for which the local alignment is weak and the particles cannot form stable clusters. Therefore, the demixing of the two types of particles and  $S$  is small. An increase in  $v_0$  can improve this situation, because a larger persistence length can provide sparse particles with more opportunities to come into proximity, enhancing interactions between particles and subsequently strengthening local alignment. When  $\Phi$  is large, the significantly small distance between particles leads to the dominance of their repulsive interactions, for which the particles are difficult to align. Thus, the same type of particles cannot gather stably and  $S \rightarrow 0$ . Note that the position of the peak of  $S$  moves towards left when  $v_0$  increases. This is because a large self-propulsion velocity implies a large circular motion radius, and the particle distribution must correspondingly become more sparse to match it, causing the particle spacing to approach the range of attractive interactions, thus favoring dominant attractive interactions.

Figure 14 displays the separation coefficient  $S$  as a function of interaction strength  $\epsilon$  at  $v_0 = 2.5$  and  $\Omega = 0.9$ . The separation coefficient is found to be a peak function of the interaction strength. When  $\epsilon$  is small, the attractive interaction

is not significant, so the two types of particles are difficult to separate. When  $\epsilon$  is large, the attractive force is very significant, and the two types of particles are indiscriminately attracted closely together, making separation impossible. Therefore, there exists an intermediate value of interaction strength at which the separation coefficient reaches its maximum value. Regarding the cutoff radius  $r_{\text{cut}}$ , it is permissible to choose a value larger than  $3\sigma$ , for example, choosing  $4\sigma$ . However, when  $r_{\text{cut}} = 3\sigma$ , the interaction between particles is already very small,  $\sim 10^{-3}\epsilon$ . Even if the range of attraction is slightly increased, it can still be predicted that the results will not differ significantly in essence. If  $r_{\text{cut}}$  is set to be  $2^{1/6}\sigma$  (only repulsive force exists), then MIPS may occur. Moreover, as the angular velocity increases from zero to a large value, MIPS may first strengthen and then weaken, potentially undergoing transitions from the homogeneous state to a MIPS state to the dynamic clustering state, ultimately returning to the homogeneous state [72].

Finally, we assessed the finite-size effects of this system, as shown in Fig. 15. When the angular velocity  $\Omega \ll 1$  (i.e.,  $R \rightarrow \infty$ ) or very large  $\Omega \rightarrow \infty$  (i.e.,  $R \rightarrow 0$ ), the influence of size effects on the separation coefficient is not significant, and the separation coefficient is very small. However, when the angular velocity takes appropriate intermediate values (in the range of  $2^{1/6}\sigma < R < 3\sigma$  where attraction dominates), the separation coefficient takes its maximum, and initially increases with increasing system size and then stabilizes.

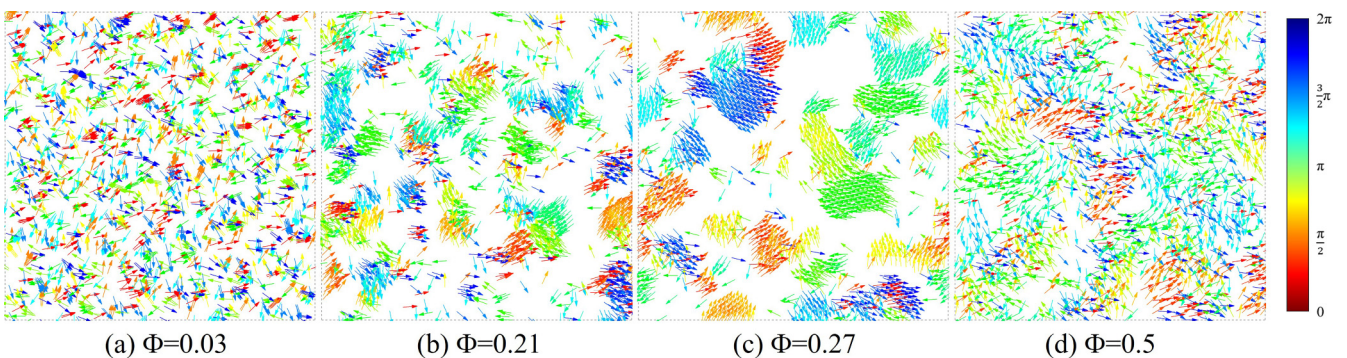


FIG. 11. The velocities of particles for typical snapshots in Fig. 10. The color on the velocity vector represents the mapping of velocity direction angles. The snapshots are all scaled from their actual sizes to a standardized image dimension.

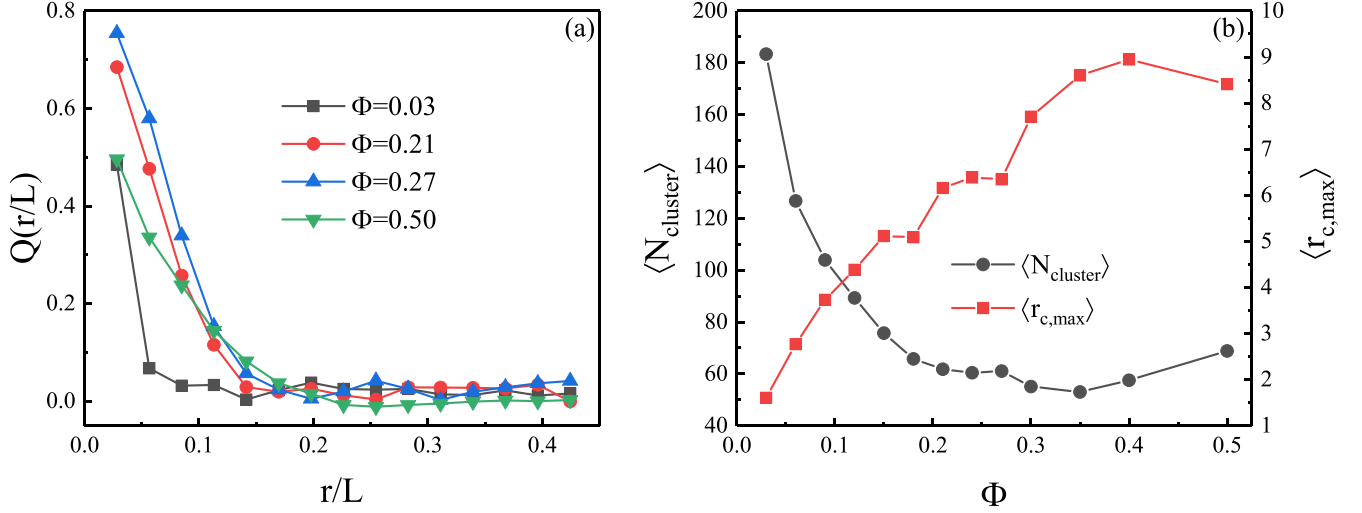


FIG. 12. (a) The spatial velocity correlation function  $Q(r/L)$  versus the distance  $r$  for typical snapshots shown in Figs. 10(a)–10(d). (b) The number of clusters and size of max cluster as functions of packing fraction  $\Phi$  at  $v_0 = 2.5$  and  $\Omega = 0.9$ .

Separation arises from local alignment caused by attractive interactions, and hence the optimal circumferential radius for achieving the largest separation coefficient does not significantly vary with size. When the system size is small, clusters are prone to boundary effects, where cluster parts can easily break away due to influence from one end far from the cluster center, resulting in instability. As size increases, the possibility of such effects decreases. Once the size is large enough that boundary effects on cluster stability can be disregarded, the separation coefficient no longer increases with size.

#### IV. CONCLUDING REMARKS

In this work, we numerically investigate the separation of a binary mixture of active chiral Brownian particles with

attractive interactions. It is found that the two types of particles can spontaneously separate without any explicit aligning interactions or other interventions. This is attributed to the ability of active Brownian particles to spontaneously generate local alignment or even global alignment under attractive interactions [26]. Particles of different chirality can form stable clusters under the aligning effect, finally leading to demixing. At very low angular velocities, the dynamical differences between the two types of particles are not significant, while particles tend to rotate in place at very high angular velocities, resulting in the separation coefficient being a peak function of angular velocity. There exists an optimal separation angular velocity, which increases with the self-propulsion speed. The separation coefficient first increases and then decreases with the self-propulsion speed, because intermediate self-propulsion speeds lead to significant dynamical differences

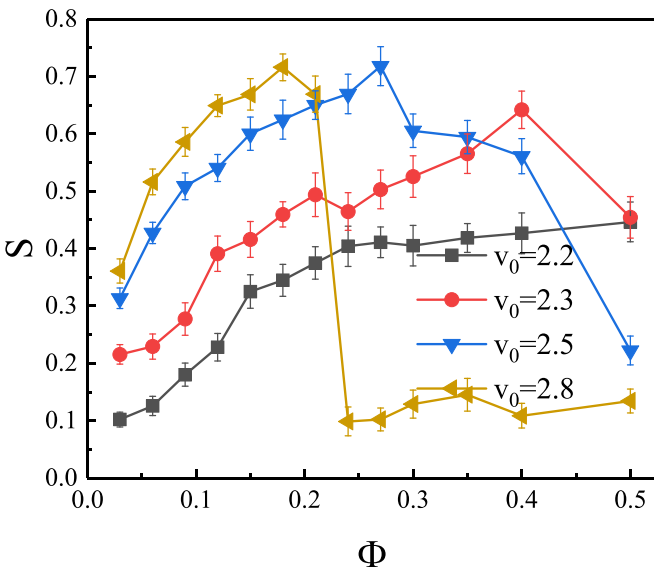


FIG. 13. Separation coefficient  $S$  as a function of packing fraction  $\Phi$  for different  $v_0$  at  $\Omega = 0.9$ .

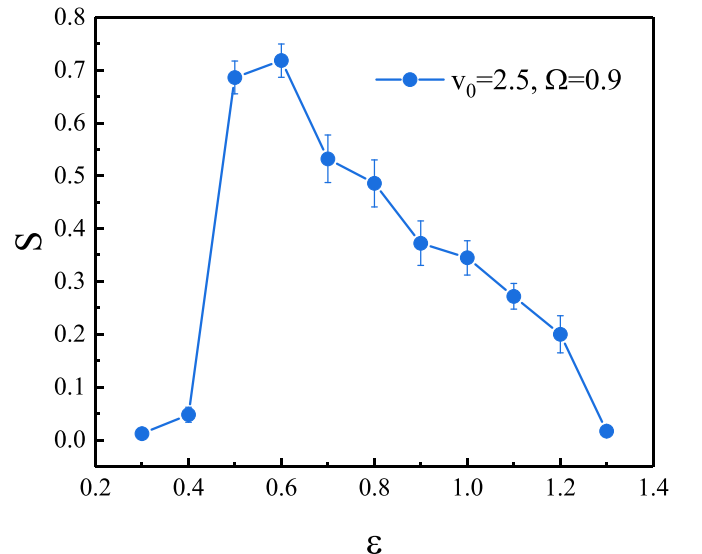


FIG. 14. Separation coefficient  $S$  as a function of interaction strength  $\epsilon$  at  $v_0 = 2.5$  and  $\Omega = 0.9$ .



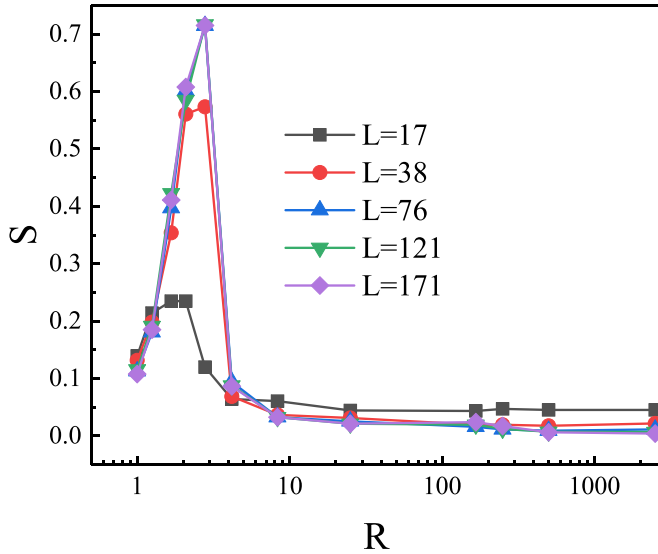


FIG. 15. Separation coefficient  $S$  as a function of radius of circular motion  $R$  at  $v_0 = 2.5$  and  $\Omega = 0.9$  for different size (corresponding to  $N = 100, 500, 2000, 5000, 10000$ , respectively).

between the particles without them easily escaping from clusters. The dominance of attractive forces requires moderate particle distance, and an intermediate packing fraction satisfies this condition, thereby making the separation coefficient a peak function of the packing fraction.

The chiral mixtures with attractive interaction is challenging to separate because of the indiscriminate attraction among particles. We propose a new mechanism for the spontaneous separation of chiral active particles with the attractive interactions between particles, which contributes to a deeper understanding of the mechanism for chiral matter separation. It is of interest that the attractive interaction among particles is incorporated into experiments [38,73,74] concerning the separation of chiral mixtures.

#### ACKNOWLEDGMENTS

This work was supported in part by the National Natural Science Foundation of China (Grant No. 12075090) and the Guangdong basic and applied basic research foundation (Grants No. 2022A1515010449 and No. 2024A1515012575).

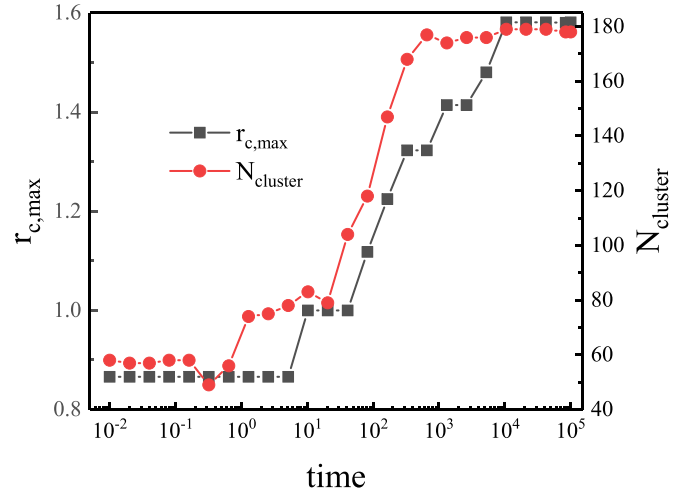


FIG. 16. The number of clusters and the size of max cluster as functions of simulation time for  $v_0 = 2.5$ ,  $\Omega = 0.9$ , and  $\Phi = 0.03$ .

#### APPENDIX: THE CALCULATION OF CLUSTERS

We only analyze clusters formed by particles of the same type (taking CCW particles as an example). There are two reasons for this: First, our primary focus is on segregation phenomena; second, the distinction between CCW and CW particles lies only in their rotational direction and does not affect the formation of their respective clusters. The number of clusters and size of the max cluster are calculated by the following steps: (i) Calculate the distance  $r_{ij}^{\text{CCW}}$  between each pair of CCW particles and (ii) judge whether  $r_{ij}^{\text{CCW}}$  satisfies  $r_{ij}^{\text{CCW}} \leq 1.5\sigma$ . If so, then particles  $i$  and  $j$  are considered to be in the same cluster and (iii) calculate the size of each cluster that each particle belongs to by using depth-first search (DFS) algorithm.

To verify that our simulation time are sufficiently long to achieve equilibrium in cluster evolution, particularly at low densities (e.g.,  $\Phi = 0.03$ ), we computed the temporal evolution of the number of clusters  $N_{\text{cluster}}$  and the size of the max cluster  $r_{c,\text{max}}$ , as shown in Fig. 16. It is observed that both  $r_{c,\text{max}}$  and  $N_{\text{cluster}}$  stabilize when simulation time more than  $10^4$ , indicating steady state in cluster evolution in our simulations. Note that angle brackets  $\langle \dots \rangle$  added to  $r_{c,\text{max}}$  and  $N_{\text{cluster}}$  elsewhere in the main text denote the average over time after steady state.

- [1] C. Bechinger, R. Di Leonardo, H. Löwen, C. Reichardt, G. Volpe, and G. Volpe, *Rev. Mod. Phys.* **88**, 045006 (2016).
- [2] Y. Li, P. K. Ghosh, F. Marchesoni, and B. Li, *Phys. Rev. E* **90**, 062301 (2014).
- [3] Y. F. He, B. Q. Ai, C. X. Dai, C. Song, R. Q. Wang, W. T. Sun, F. C. Liu, and Y. Feng, *Phys. Rev. Lett.* **124**, 075001 (2020).
- [4] C. Grossert, M. Leder, S. Denisov, P. Hänggi, and M. Weitz, *Nat. Commun.* **7**, 10440 (2016).
- [5] P. K. Ghosh, V. R. Misko, F. Marchesoni, and F. Nori, *Phys. Rev. Lett.* **110**, 268301 (2013).
- [6] P. K. Ghosh, P. Hänggi, F. Marchesoni, and F. Nori, *Phys. Rev. E* **89**, 062115 (2014).
- [7] F. Kümmel, B. ten Hagen, R. Wittkowski, I. Buttinoni, R. Eichhorn, G. Volpe, H. Löwen, and C. Bechinger, *Phys. Rev. Lett.* **110**, 198302 (2013).
- [8] M. B. Wan, C. J. Olson Reichardt, Z. Nussinov, and C. Reichardt, *Phys. Rev. Lett.* **101**, 018102 (2008).
- [9] B. Q. Ai, J. Ma, C. H. Zeng, and Y. F. He, *Phys. Rev. E* **107**, 024406 (2023).
- [10] B. Ai, *Phys. Rev. E* **108**, 064409 (2023).
- [11] C. J. Olson Reichardt and C. Reichardt, *Annu. Rev. Condens. Matter Phys.* **8**, 51 (2017).
- [12] E. Putzig and A. Baskaran, *Phys. Rev. E* **90**, 042304 (2014).
- [13] E. Mani and H. Löwen, *Phys. Rev. E* **92**, 032301 (2015).

- [14] M. E. Cates and J. Tailleur, *Annu. Rev. Condens. Matter Phys.* **6**, 219 (2015).
- [15] Y. Fily and M. C. Marchetti, *Phys. Rev. Lett.* **108**, 235702 (2012).
- [16] L. Berthier, E. Flenner, and G. Szamel, *J. Chem. Phys.* **150**, 200901 (2019).
- [17] E. Flenner, G. Szamel, and L. Berthier, *Soft Matter* **12**, 7136 (2016).
- [18] T. Vicsek, A. Czirók, E. Ben-Jacob, I. Cohen, and O. Shochet, *Phys. Rev. Lett.* **75**, 1226 (1995).
- [19] J. Zhang, R. Alert, J. Yan, N. S. Wingreen, and S. Granick, *Nat. Phys.* **17**, 961 (2021).
- [20] H. Chaté, F. Ginelli, G. Grégoire, and F. Raynaud, *Phys. Rev. E* **77**, 046113 (2008).
- [21] A. Martín-Gómez, D. Levis, A. Díaz-Guilera, and I. Pagonabarraga, *Soft Matter* **14**, 2610 (2018).
- [22] M. N. van der Linden, L. C. Alexander, D. G. A. L. Aarts, and O. Dauchot, *Phys. Rev. Lett.* **123**, 098001 (2019).
- [23] E. Sesé-Sansa, G. J. Liao, D. Levis, I. Pagonabarraga, and S. H. L. Klapp, *Soft Matter* **18**, 5388 (2022).
- [24] M. Pu, H. Jiang, and Z. Hou, *Soft Matter* **13**, 4112 (2017).
- [25] T. Vicsek and A. Zafeiris, *Phys. Rep.* **517**, 71 (2012).
- [26] L. Caprini and H. Löwen, *Phys. Rev. Lett.* **130**, 148202 (2023).
- [27] K. Maeda, Y. Imae, J. I. Shioi, and F. Oosawa, *J. Bacteriol.* **127**, 1039 (1976).
- [28] W. R. DiLuzio, L. Turner, M. Mayer, P. Garstecki, D. B. Weibel, H. C. Berg, and G. M. Whitesides, *Nature (London)* **435**, 1271 (2005).
- [29] E. Lauga, W. R. DiLuzio, G. M. Whitesides, and H. A. Stone, *Biophys. J.* **90**, 400 (2006).
- [30] E. P. Ipina, S. Otte, R. Pontier-Bres, D. Czerucka, and F. Peruani, *Nat. Phys.* **15**, 610 (2019).
- [31] P. Patra, K. Beyer, A. Jaiswal, A. Battista, K. Rohr, F. Frischknecht, and U. S. Schwarz, *Nat. Phys.* **18**, 586 (2022).
- [32] I. H. Riedel, K. Kruse, and J. Howard, *Science* **309**, 300 (2005).
- [33] Y. Yang, J. Elgeti, and G. Gompper, *Phys. Rev. E* **78**, 061903 (2008).
- [34] J. Elgeti, R. G. Winkler, and G. Gompper, *Rep. Prog. Phys.* **78**, 056601 (2015).
- [35] F. Afroze, D. Inoue, T. I. Farhana, T. Hiraiwa, R. Akiyama, A. M. R. Kabir, K. Sada, and A. Kakugo, *Biochem. Biophys. Res. Commun.* **563**, 73 (2021).
- [36] Y. Shelke, N. R. Srinivasan, S. P. Thampi, and E. Mani, *Langmuir* **35**, 4718 (2019).
- [37] L. Alvarez, M. A. Fernandez-Rodriguez, A. Alegria, S. Arrese-Igor, K. Zhao, M. Kröger, and L. Isa, *Nat. Commun.* **12**, 4762 (2021).
- [38] T. Barois, J. F. Boudet, J. S. Lintuvuori, and H. Kellay, *Phys. Rev. Lett.* **125**, 238003 (2020).
- [39] P. Arora, A. K. Sood, and R. Ganapathy, *Sci. Adv.* **7**, eabd0331 (2021).
- [40] J. Mecke, J. O. Nketsiah, R. Li, and Y. Gao, *Natl. Sci. Open* **3**, 20230086 (2024).
- [41] B. C. van Zuiden, J. Paulose, W. T. Irvine, D. Bartolo, and V. Vitelli, *Proc. Natl. Acad. Sci. USA* **113**, 12919 (2016).
- [42] S. van Teeffelen and H. Löwen, *Phys. Rev. E* **78**, 020101(R) (2008).
- [43] B. Liebchen, M. E. Cates, and D. Marenduzzo, *Soft Matter* **12**, 7259 (2016).
- [44] P. Liu, H. Zhu, Y. Zeng, G. Du, L. Ning, D. Wang, K. Chen, Y. Lu, N. Zheng, F. Ye, and M. Yang, *Proc. Natl. Acad. Sci. USA* **117**, 11901 (2020).
- [45] B. Liebchen and D. Levis, *Phys. Rev. Lett.* **119**, 058002 (2017).
- [46] L. Caprini and U. M. B. Marconi, *Soft Matter* **15**, 2627 (2019).
- [47] F. J. Sevilla, *Phys. Rev. E* **94**, 062120 (2016).
- [48] X. Yang, C. Ren, K. Cheng, and H. P. Zhang, *Phys. Rev. E* **101**, 022603 (2020).
- [49] C. Reichhardt and C. J. O. Reichhardt, *Phys. Rev. E* **100**, 012604 (2019).
- [50] J. Mecke, Y. Gao, C. A. R. Medina, D. G. A. L. Aarts, G. Gompper, and M. Ripoll, *Commun. Phys.* **6**, 324 (2023).
- [51] D. Banerjee, A. Souslov, A. G. Abanov, and V. Vitelli, *Nat. Commun.* **8**, 1573 (2017).
- [52] N. Kruk, J. A. Carrillo, and H. Koepl, *Phys. Rev. E* **102**, 022604 (2020).
- [53] G. Kokot, S. Das, R. G. Winkler, G. Gompper, I. S. Aranson, and A. Snezhko, *Proc. Natl. Acad. Sci. USA* **114**, 12870 (2017).
- [54] Q. Lei, M. P. Ciamarra, and R. Ni, *Sci. Adv.* **5**, eaau7423 (2019).
- [55] D. Levis and B. Liebchen, *Phys. Rev. E* **100**, 012406 (2019).
- [56] D. Levis, I. Pagonabarraga, and B. Liebchen, *Phys. Rev. Res.* **1**, 023026 (2019).
- [57] B. Q. Ai, Z. G. Shao, and W. R. Zhong, *Soft Matter* **14**, 4388 (2018).
- [58] C. Scholz, M. Engel, and T. Pöschel, *Nat. Commun.* **9**, 931 (2018).
- [59] N. H. P. Nguyen, D. Klotsa, M. Engel, and S. C. Glotzer, *Phys. Rev. Lett.* **112**, 075701 (2014).
- [60] J. M. Moore, M. A. Glaser, and M. D. Betterton, *Soft Matter* **17**, 4559 (2021).
- [61] K. Yeo, E. Lushi, and P. M. Vlahovska, *Phys. Rev. Lett.* **114**, 188301 (2015).
- [62] M. Mijalkov and G. Volpe, *Soft Matter* **9**, 6376 (2013).
- [63] C. Reichhardt and C. J. Olson Reichhardt, *Phys. Rev. E* **88**, 042306 (2013).
- [64] A. Nourhani, V. H. Crespi, and P. E. Lammert, *Phys. Rev. Lett.* **115**, 118101 (2015).
- [65] Marcos, H. C. Fu, T. R. Powers, and R. Stocker, *Phys. Rev. Lett.* **102**, 158103 (2009).
- [66] P. Bag, S. Nayak, T. Debnath, and P. K. Ghosh, *J. Phys. Chem. Lett.* **13**, 11413 (2022).
- [67] B. Q. Ai, S. Quan, and F. G. Li, *New J. Phys.* **25**, 063025 (2023).
- [68] E. N. Tsiok, Y. D. Fomin, E. A. Gaiduk, E. E. Tareyeva, V. N. Ryzhov, P. A. Libet, N. A. Dmitryuk, N. P. Kryuchkov, and S. O. Yurchenko, *J. Chem. Phys.* **156**, 114703 (2022).
- [69] Y. J. Chiu and A. K. Omar, *J. Chem. Phys.* **158**, 164903 (2023).
- [70] P. Sahu, D. M. Sussman, M. Rübsam, A. F. Mertz, V. Horsley, E. R. Dufresne, C. M. Niessen, M. Cristina Marchetti, M. Lisa Manninga, and J. M. Schwarz, *Soft Matter* **16**, 3325 (2020).
- [71] L. Caprini, U. Marini Bettolo Marconi, and A. Puglisi, *Phys. Rev. Lett.* **124**, 078001 (2020).
- [72] Z. Ma and R. Ni, *J. Chem. Phys.* **156**, 021102 (2022).
- [73] C. W. Chan, D. Wu, K. Qiao, K. L. Fong, Z. Yang, Y. Han, and R. Zhang, *Nat. Commun.* **15**, 1406 (2024).
- [74] L. Fang and J. Wang, *Phys. Rev. Lett.* **127**, 233902 (2021).